Excess Carrier Concentration in Silicon Devices and Wafers: How Bulk Properties are Expected to Accelerate Light and Elevated Temperature Degradation

A.N. McPherson, J.F. Karas, D.L. Young, I.L. Repins
National Renewable Energy Laboratory

Abstract

Light and elevated temperature induced degradation (LeTID) is accelerated nearly linearly by the presence of excess carriers. It is therefore important to understand how excess carrier concentration (Δn) changes as a function of exposure conditions, materials properties, and sample structure. We simulate Δn as a function of wafer thickness and bulk minority carrier lifetime (τ) in solar cells and wafers using SCAPS and Quokka3. We also derive closed-form analytic expressions. For wafers, there is a near-linear relationship between Δn and τ or thickness, whereas for solar cells, Δn in the bulk may become limited by rear surface recombination. Thus, LeTID may progress more quickly in wafers than in cells, with a stronger dependence on τ. When comparing experiments, observed degradation rates must be corrected between samples or conditions to account for differences in Δn. This study demonstrates three tools to estimate the magnitude of such corrections, which can aid in the quantitative interpretation of LeTID data and performance predictions. While each tool yields similar results, there are advantages to each approach that must be weighed in terms of simplicity of inputs versus sophistication of treatment. Incomplete specification of back contact characteristics in commercial products is identified as an important contributor to uncertainty in expected LeTID rates.

1. Introduction and Goals

Predicting degradation rates of fielded modules is important to understanding energy yield, return on investment, and the value of eradicating certain types of degradation. Such evaluations are made both on modules that are already installed in the field and on new products. Diagnosis of problems in fielded modules often lags behind laboratory experience, as abnormal degradation is sometimes apparent only after several years of steady decline in performance, with changes large enough to be separated from weather, soiling, and other effects. At that time system owners and researchers begin to pinpoint the root cause of degradation and how to test for the effect in future modules. For example, although LeTID was first reported in laboratory tests in 2012 [1], the first published report of LeTID diagnosed in a utility-scale system did not appear until 2020 [2], and an IEC standard to test for LeTID in modules is expected to be published in 2023 [3]. Thus, diagnostic techniques are most useful if they are applicable to a variety of product types. For the case of LeTID, degradation and regeneration are accelerated by excess carriers. It is therefore important to understand how Δn changes as a function of the variety test conditions and material properties that one may

encounter in the laboratory and in the field. In the literature, experiments have been performed on modules [1-6], solar cells [7,8], and wafers [9-11] to evaluate the LeTID process kinetics. In some cases, conditions have been controlled to maintain a constant and known Δn [12], but often in these experiments Δn is unknown.

Possible consequences of interpreting degradation rates without accounting for Δn are illustrated in Figure 1. Accelerated test data from two commercial modules are shown. Current was applied at elevated temperatures, following test conditions commonly used for LeTID and subsequent regeneration [13]. In the first step (not shown), the modules were stressed to induce LeTID by applying current of I_{sc} - I_{mp} (i.e. the one-sun short circuit minus the one-sun maximum power current) at 75 °C. Next, in the regeneration phase of the test, shown Figure 1, a current of Isc was applied at 85 °C. Judging by the time to reach 50% regeneration, the mono-Si PERC module recovers approximately 4x faster than the multi-Si Al BSF module. This difference in rates might lead one to conclude that the LeTID defect is different in mono-Si than in multi-Si. However, we will show that Δn in the PERC module is expected to be about 4x higher than in the Al BSF module. Thus, the dominant effect is likely the difference in Δn rather than in the underlying defect properties.

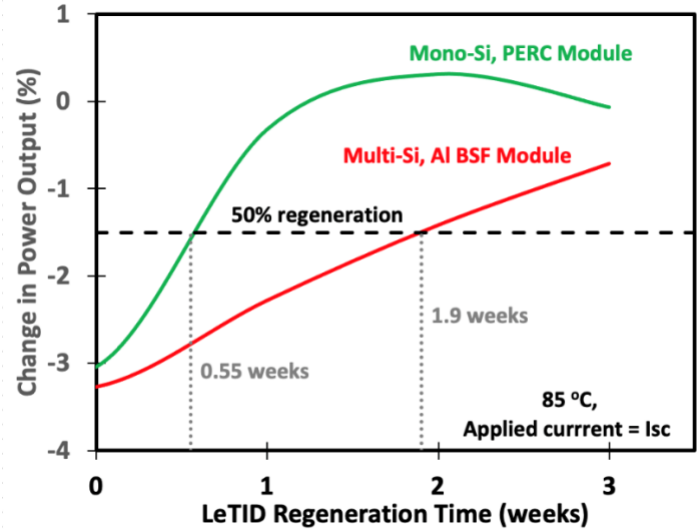

Figure 1: Accelerated test data from two commercial modules. The mono-Si passivated emitter and rear contact (PERC) cell is shown in green. The multi-Si Al back surface field (BSF) cell is shown in red.

In this paper, we examine how Δn changes as a function of τ and thickness for both illuminated solar cells and wafers at V_{OC}. Bulk thickness was varied from 50 µm to 500 µm, to span the extremes that might be studied, from flexible Si cells (50 µm) [14], to older laboratory devices (450 µm) [15]. A wide range of τ, from 10 to 1000 µs, was also examined. This range encompasses Si that has undergone severe LeTID [10] to float-zone Si, which is sometimes used in LeTID studies [12]. We compare results from SCAPS, and Quokka3, and analytic expressions.

2. Modeling Method and Inputs

Modeling was performed in both SCAPS [16] and Quokka3 [17] software. Quokka3 is commonly used for silicon solar cells and allows 3D modeling. Boundary conditions are set using a skin

approximation [18]. SCAPS allows setting the device features more generally, but only in 1D. Interfaces can be engineered in terms of band offsets, trapped charge, and interface recombination velocity. For either package, inputs were set as described in Fell [19] for PERC cells, except where noted otherwise. Key parameters in [19] for PERC cells are active dopant density of 10^{16} cm^{-3} and electron lifetime of 371 μs in the bulk, and rear surface recombination velocity in the passivated (metalized) areas of 10^5 (10^7) cm/sec. The operating point for simulations was set to open-circuit, as this is a common laboratory LeTID test condition, and we wish to compare cell and wafer results, the latter being necessarily at open circuit. However, it is also possible to run the models at other conditions (e.g. I_{mp}).

The description of back surface recombination is necessarily different when using a 3D or 1D model. When utilizing a 3D model (e.g. Quokka3), the PERC back contact is described rigorously by specifying two separate surface recombination velocities (S): one for the metalized areas (S_{met}) and one for the passivated area (S_{pass}). Doping profiles and trapped charge in the vicinity of the metallized and passivated areas are also described separately. However, a 1D model can only rigorously describe a solar cell with essentially planar features (e.g. Al BSF). For use with a 1D model, the PERC cell back contact must thus be approximated by 1D effective parameters [20,21]. For SCAPS, the required input is the effective back surface recombination velocity (S_{eff}), so the recombination characteristics of the multi-dimensional PERC back contact were converted to a 1D effective value for SCAPS using the method of Saint-Cast [21,22] for 14% back contact metal coverage [19].

Multi-dimensional, optical properties —such as busbar shading and texturing—were ignored because of their relatively small effect on Δn compared to τ , thickness, or back contact characteristics. While optical properties may cause several percent change in absorption, this study is examining much larger changes in Δn (e.g. 100x).

The wafer is modeled with the same parameters as the p-Si bulk layer from the solar cell. Many options exist for surface passivation of wafers [23], particularly for laboratory measurements, where manufacturing constraints on layer cost and throughput are removed. The limiting case of no surface recombination is modeled in this study.

Bulk carrier density profile is an output of the modeling software. The Δn profile was reduced to a spatially weighted average over the quasi-neutral region, $\overline{\Delta n}$. For SCAPS, this average was performed to within 0.1 μm of the p-bulk edge, to avoid impacts on the average from the rear p++ space charge region. For Quokka3, where only 14% of the rear surface is covered by metallic contacts and the associated space charge regions, averaging was performed over the entire p-bulk thickness.

3. Modeling Results

Figure 2 illustrates $\overline{\Delta n}$, obtained from varying thickness or τ. The discrete points show the value at which the calculations were performed, connected by a line to guide the eye. Results

obtained from Quokka3 are shown as solid lines, and those from SCAPS are shown as dashed lines. $\overline{\Delta n}$ increases with τ. As diffusion length approaches and exceeds the bulk thickness, the effect of S dominates, causing the traces to flatten for higher τ, most dramatically for the thinner cells. At a fixed τ, $\overline{\Delta n}$ decreases with thickness, because the carriers are spread over a larger width.

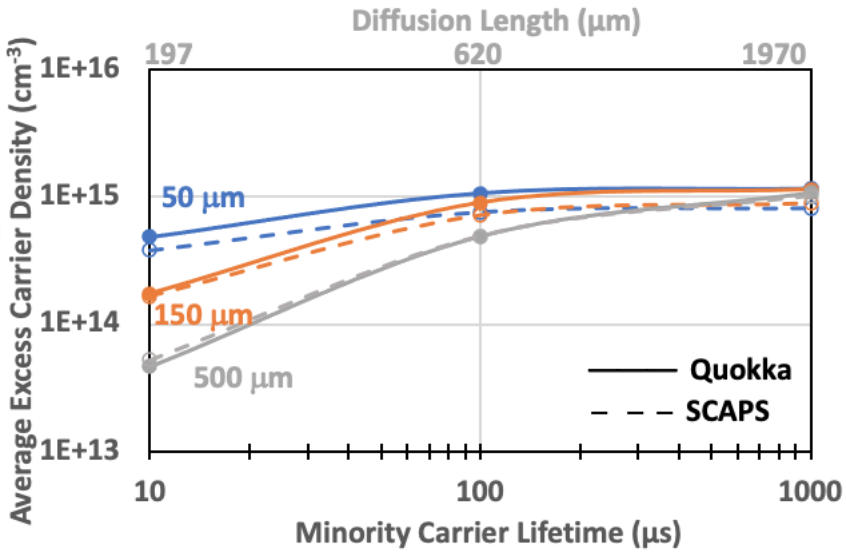

Figure 2: Modeling results from Quokka3 and SCAPS describing the relationship between $\overline{\Delta n}$ and varying bulk thickness or τ.

Figure 2 also allows us to compare the results from SCAPS versus Quokka3. The two software packages yield similar values for $\overline{\Delta n}$, with disagreement ranging from less than 1% to 29%, depending on the conditions modeled. Disagreement is largest where diffusion length is large relative to thickness. Under these conditions, an accurate description of the back contact is most important, and SCAPS underestimates $\overline{\Delta n}$ compared to Quokka. This underestimation is consistent with our use of an upper-limit 1D S_{eff}, related to the method of Saint-Cast [21,22].

Figure 3 uses SCAPS to compare cell and wafer results. For the wafers, $\overline{\Delta n}$ increases proportionally with τ. This linear increase is different than behavior in the cell, where $\overline{\Delta n}$ barely increases with τ, once carriers can diffuse easily to the back contact. Figure 3 shows that for a typical PERC cell (τ = 400 µs, t~180 µm) $\overline{\Delta n}$, and therefore degradation rate, in the wafer vs. solar cell are expected to differ by a factor of 10, even for identical bulk and defect properties.

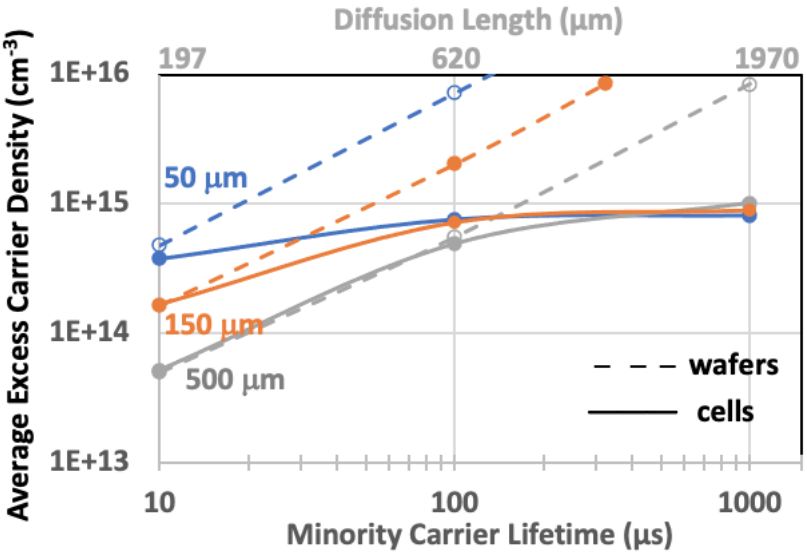

Figure 3: $\overline{\Delta n}$ in the p-bulk for a range of wafer thickness and τ, for both passivated wafers and PERC solar cells.

4. Analysis Based on Device Physics Equations

Simplified analytic expressions for $\overline{\Delta n}$ are convenient for lengthy calculations that aim to predict defect populations over the course of years of outdoor exposure in fielded modules. Such analytic expressions are obtained starting with the solution to the minority carrier diffusion equation in the p-type quasi-neutral region (QNR) [24], for a diode with applied voltage in low injection:

$$\Delta n(x) = A_p \sinh\left(\frac{x-x_p}{\sqrt{D\tau}}\right) + B_p \cosh\left(\frac{x-x_p}{\sqrt{D\tau}}\right) \quad \text{(i)}$$

where

$$A_p \equiv -\frac{\frac{n_i^2}{N_a} e^{qV/kT}\left[\frac{S_{eff}}{D}\cosh\left(\frac{W-x_p}{\sqrt{D\tau}}\right)+\left(\frac{1}{\sqrt{D\tau}}\right)\sinh\left(\frac{W-x_p}{\sqrt{D\tau}}\right)\right]}{\left(\frac{1}{\sqrt{D\tau}}\right)\cosh\left(\frac{W-x_p}{\sqrt{D\tau}}\right)+\left(\frac{S_{eff}}{D}\right)\sinh\left(\frac{W-x_p}{\sqrt{D\tau}}\right)} \quad \text{(ii)}$$

$$B_p \equiv \frac{n_i^2}{N_a} e^{qV/kT} \quad \text{(iii)}$$

and other variables are defined as in Table 1.

Variable	Quantity	Units	Variable	Quantity	Units
Δn	Excess electron density	m^{-3}	q	Electron charge	coul
x	Distance into p-layer	m	V	Applied voltage	volts
x_p	Thickness of SCR in p-Si	m	k	Boltzmann's constant	Joule/K
D	Diffusion coefficient	m^2/sec	T	Temperature	K
τ	Electron lifetime	m	S_{eff}	Effective back surface recombination velocity	m/sec
n_i	Intrinsic carrier density	m^{-3}	W	P-layer thickness	m
N_a	Acceptor density	m^{-3}			

Table 1: Definition of variables, following [24].

Integrating eq. (i) over the QNR yields an expression for the $\overline{\Delta n}$ in the QNR:

$$\overline{\Delta n} = \frac{\sqrt{D\tau}}{W-x_P}\left\{A_p\left[\cosh\left(\frac{W-x_p}{\sqrt{D\tau}}\right)-1\right] + B_p \sinh\left(\frac{W-x_p}{\sqrt{D\tau}}\right)\right\} \quad \text{(iv)}$$

Using eq. (iv) requires specifying an applied voltage, which was chosen to be the open-circuit voltage, V_{oc}. V_{oc} is related to the diode saturation current density (J_0) and the short-circuit current density (J_{sc}) via

$$Voc = \frac{kT}{q}\, ln\left[\frac{J_{sc}}{J_o}\right] \quad \text{(v)}$$

where

$$Jo = q\,\frac{n_i^2}{N_a}\,\sqrt{\frac{D}{\tau}}\,\frac{\sqrt{\frac{D}{\tau}}\sinh\left[\frac{W-x_P}{\sqrt{D\tau}}\right]+S_{eff}\cosh\left[\frac{W-x_P}{\sqrt{D\tau}}\right]}{\sqrt{\frac{D}{\tau}}\cosh\left[\frac{W-x_P}{\sqrt{D\tau}}\right]+S_{eff}\sinh\left[\frac{W-x_P}{\sqrt{D\tau}}\right]} \quad \text{(vi)}$$

Equation (vi) does not assume a long base in its derivation [25]. Also, although analysis in this study is performed at open-circuit, eq. (iv) may be evaluated at any voltage to calculate $\overline{\Delta n}$ at other operating points.

The same materials values used for numerical modeling can be plugged into eq. (iv). For parameters S_{eff} and J_{sc}, some assumptions must be made. First, the diode equation does not account for impact of both the p++ back surface field and recombination at the rear interface. Thus, for S_{eff} in equation (ii), we use the effective combined value of 90 cm/sec, as measured on PERC cells by Gatz [26]. Second, as J_{sc} can depend on complex multi-dimensional optical effects which are outside the scope of this paper, we simply use 40 mA/cm^2.

For a passivated wafer, a simple expression results if one assumes a uniform Δn, i.e. diffusion length is long enough to prevent non-uniform generation from creating substantial gradients in Δn. In this case, the recombination per volume $\frac{\Delta n}{\tau}$ must be equal to the generation per volume $\frac{J}{W}$, yielding

$$\Delta n = \frac{J\,\tau}{W} \quad \text{(vii)}$$

The results of calculations using equations (iv) and (vii) are shown in Figure 4. Results are nearly identical to those obtained earlier using SCAPS (Figure 3).

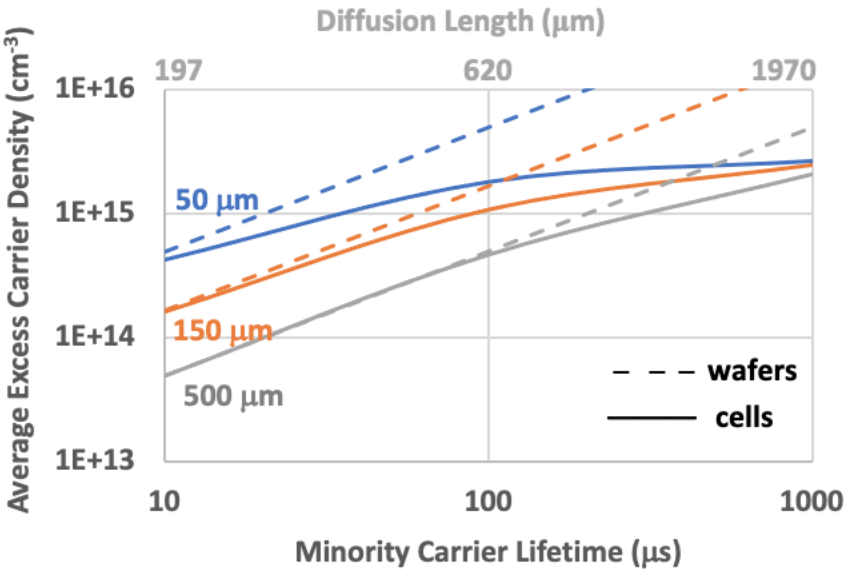

Figure 4: $\overline{\Delta n}$ calculated via closed-form analytic expressions for a range of thicknesses.

5. Discussion

A number of physical effects related to photovoltaic reliability are known to accelerate with Δn. Such effects include BO LID, where the regeneration rate has been shown to be linear with injected carrier density [27], and LeTID, where degradation and regeneration processes have been observed to be accelerated approximately linearly with carrier injection [28,29]. The calculations in this paper show that when the same conditions are applied to samples with different characteristics, the resulting Δn is different, and thus degradation rates will be different. In fact, an increase in LeTID rates for thinner wafers has been observed experimentally [30-32], although multiple factors are likely at play. There appears to be a lower defect concentration in thinner wafers due to faster defect diffusion to the edges during processing, a higher Δn due to the lower defect concentration, and a higher Δn due to confining carriers into a thinner wafer.

Results indicate that τ and S are important inputs in the estimation of $\overline{\Delta n}$. These parameters may be unknown, particularly for commercial modules. While typical values for a given cell type may be assumed, the range of τ reported for commercial PERC cells (100-500 μs), at a typical 180 μm solar cell thickness, can cause a factor of two variation in $\overline{\Delta n}$ and thus related degradation rates. $\overline{\Delta n}$ in high-lifetime PERC cells is predicted to be even more sensitive to variations in S. For commercial modules, even where τ and S may be estimated from detailed measurements on a single cell or module, it is unclear how τ and S change between power classes, or for different bills of materials included within a single power class. Even within a single wafer, inhomogeneity of defect concentrations may lead to spatial variations in τ, $\overline{\Delta n}$, and thus defect transition rates [33]. These hidden variations in $\overline{\Delta n}$ likely account for some portion of the disagreement in kinetic behavior [4, 11] observed for LeTID.

The equations and modeling in this paper provide three options for tools to correct for variations in properties across data sets, or at least establish limits of error based on the possible resulting variations in Δn. Quokka3 excels in its ability to treat the 3D nature of the back contact rigorously. SCAPS allows setting device features more generally, but only in 1D, and thus requires treating the back contact with an S_{eff} approximation. For typical PERC cell parameters, use of an upper-limit S_{eff} causes underestimated of $\overline{\Delta n}$ by 30%. Use of analytic expressions is convenient for numerical modeling of performance versus time, but also requires deriving an approximate S_{eff}.

We can use these learnings to understand the different LETID regeneration rates in Figure 1. Specifically, using equations (iv) – (vi) with values typical for Al BSF (τ = 75 μs, S = 500 cm/sec), we obtain $\overline{\Delta n}_{Al\ BSF}$= 4.6 x 10^{14} cm^{-3}. Using typical values for PERC cells (τ = 370 μs, S = 90 cm/sec), we obtain $\overline{\Delta n}_{PERC}$= 1.9 x 10^{15} cm^{-3}, 4.1 times larger than in the Al-BSF cell. Thus, the ~4x rate difference observed in Figure 1 should be attributed mostly to the effects of Δn rather than a difference in defect properties.

6. Conclusions

This study elucidates how Δn in silicon devices and wafers depends on bulk properties. This quantification can help us interpret or predict LeTID transition rates, which are known to depend almost linearly on Δn. Comparable estimates of $\overline{\Delta n}$ are obtained whether one uses 3D modeling software, 1D modeling software, or analytic expressions. While increasing τ or decreasing bulk layer thickness always increases $\overline{\Delta n}$, the increase is limited by recombination at the cell back surface. Thus, processes that depend on Δn are likely to proceed faster in passivated wafers than in cells, especially in thinner wafers. Processes that depend on Δn will proceed at different rates in solar cells with different τ or back contact characteristics, which will result in apparent different kinetic parameters for a single defect if the impacts of Δn are ignored. This paper demonstrates three possible tools useful for estimating $\overline{\Delta n}$ and thus degradation rates.

Acknowledgement

This work was authored in part by the National Renewable Energy Laboratory, operated by Alliance for Sustainable Energy, LLC, for the U.S. Department of Energy (DOE) under Contract No. DE-AC36-08GO28308. Funding provided by U.S. Department of Energy Office of Energy Efficiency and Renewable Energy Solar Energy Technologies Office. The views expressed in the article do not necessarily represent the views of the DOE or the U.S. Government. The U.S. Government retains and the publisher, by accepting the article for publication, acknowledges that the U.S. Government retains a nonexclusive, paid-up, irrevocable, worldwide license to publish or reproduce the published form of this work, or allow others to do so, for U.S. Government

purposes. This material is based upon work supported by the U.S. Department of Energy's Office of Energy Efficiency and Renewable Energy (EERE) under Solar Energy Technologies Office (SETO) Agreement Number 34357.

On behalf of all authors, the corresponding author states that there is no conflict of interest.

The datasets generated during and/or analyzed during the current study are available from the corresponding author on reasonable request.

References

1. K. Ramspeck, S. Zimmerman, H. Nagel, A. Metz, Y. Gassenbauer, B. Birkmann, A. Seidl, Proc. EUPVSEC **27,** 861 (2012)
2. M. G. Deceglie, T.J. Silverman, S.W. Johnston, J.A Rand, M.J. Reed, R. Flottemesch, I.L. Repins, IEEE JPV **10** (4), 1084 (2020)
3. IEC TS 63342 ED1 "Light and elevated temperature induced degradation (LeTID) test for c-Si Photovoltaic (PV) modules: Detection," currently in translation of draft technical specification (TDTS) phase within the IEC.
4. E. Fokuhl, T. Naeem, A. Schmid, P. Gebhardt, T. Geipel, D. Philipp, Proc. EUPVSEC Conference and Exhibition **36**, 4BO122 (2019)
5. F. Kersten, F. Fertig, K. Petter, B. Kloter, E. Herzog, M.B. Strobel, J. Heitmann, J.W. Muller, Energy Procedia **124**, 540 (2017)
6. K. Nakayashiki, J. Hofstetter, A.E. Morishige, T.-T.A. Li, D. B. Needleman, M.A. Jensen, T. Buonassisi, IEEE JPV, **6**(4), 860 (2016)
7. A. Herguth, C. Derricks, P. Keller, B. Terheiden, Energy Procedia **127**, 740 (2017)
8. Z. Hu, Q. He, S. Yuan, D. Lin, L. Song, X. Yu, D. Yang, Sol. RRL **5**(7), 2100035 (2021)
9. D. Bredemeier, D. Walter, J. Schmidt, Sol. En. Mat. Sol. Cells **173**, 2 (2017)
10. F. Kersten, J. Heitmann, J.W. Müller, Proc. EUPVSEC Conference and Exhibition **32**, 507 (2016)
11. G.M. Wyller , M.S. Wiig , I. Due-Sørensen , R. Søndenå, IEEE JPV **11**(4), 878 (2021)
12. A. Graf, A. Herguth, G. Hahn, AIP Conf. Proc. **2147**, 140003 (2019)
13. J. Karas, I. Repins, M. B. Koentopp, F. Kersten, J.-N. Jaubert, C. Monokroussos, L. Jakisch, M. Pravettoni, S. Wendlandt, M. Caccivio, G. Bellenda, A. K. Tripathi, C. Banerjee, B. Bora, M. Pander, B. Jäckel, and E. Fokuhl, First Results from the International Round Robin Study on Light and Elevated Temperature Degradation, https://www.youtube.com/watch?v=zp0QA3Yn1U8&t=2929s. Accessed November 5, 2021
14. A.W.Blakers, T.Armour, Sol. En. Mat. Sol. Cells **93**(8), 1440 (2009)
15. M. A. Green, Prog. PV: Res. Appl. **17**, 183 (2009)
16. M. Burgelman, P. Nollet, S. Degrave, Thin Sol. Films, **361-362**, 527 (2000)
17. A. Fell, IEEE Trans. Elec. Dev., **60**(2), 733 (2013)
18. A. Fell, J. Schön, M. Schubert, S. Glunz, Stefan. Sol. En. Mat. Sol. Cell **173**, 128 (2017)

19. A. Fell, K.R. McIntosh, P.P. Altermatt, G.J. M. Janssen, R. Stangl, A. Ho-Baillie, H. Steinkemper, J. Greulich, M. Muller, B. Min, K.C. Fong, M. Hermle, I.G. Romijn, M.D. Abbott, IEEE JPV, **5**(4), 1250 (2015)
20. K.R. McIntosh, L.E. Black, J. Appl. Phys, **116**, 014505 (2014)
21. P. Saint-Cast, M. Rüdiger, A. Wolf, M. Hofmann, J. Rentsch, R. Preu, J. Appl. Phys **108**, 013705 (2010)
22. P. Saint-Cast, "Passivation of Si Surfaces by PECVD Aluminum Oxide," PhD Thesis, Universität Konstanz, College of Natural Sciences, July 2012
23. J. Schmidt, R/ Peibst, R. Brendel, Sol. En. Mat. Sol. Cells **187**, 39, (2018)
24. J.L. Gray, in Handbook of Photovoltaic Science and Engineering, ed. by A. Luque S. Hegedus, (John Wiley & Sons, West Sussex, 2003) Chapter 3, https://doi.org/10.1002/0470014008.ch3
25. Ibid, equation 3.128.
26. S. Gatz, J. Müller, T. Dullweber, R. Brendel, Energy Procedia **27**, 95 (2012)
27. V. Steckenreiter, D.C. Walter, J. Schmidt, AIP Adv. **7**, 035305 (2017).
28. G. M. Wyller, M. S. Wiig , I. Due-Sørensen , R. Søndenå, IEEE JPV **11**, 4, (2021).
29. W. Kwapil, T. Niewelt, M.C. Schubert, Sol. En. Mat. Sol. Cells **173**, 80 (2017)
30. D. Bredemeier, D.C. Walter, J. Schmidt, Sol. RRL **2**, 1700159 (2018)
31. D. Bredemeier, D.C. Walter, S. Herlufsen, J. Schmidt, AIP Adv. **6**, 035119 (2016)
32. U. Varshney , M. Kim , M.U. Khan , P. Hamer, C. Chan , M. Abbott, B. Hoex, IEEE JPV **11**, 1, (2021)
33. D. Skorka, A. Zuschlag, G. Hahn, Proc. EU PVSEC **32**, http://dx.doi.org/10.4229/EUPVSEC20162016-2AV.1.26 (2016)